

Measurements of the CKM angle γ at LHCb

Wojciech Krupa on behalf of LHCb collaboration

AGH University of Science and Technology al. Mickiewicza 30 30-059 Krakow Poland.

Received 3 January 2022; accepted 1 April 2022

Tree-level measurement of the CKM γ is one of the most important test of the CP violation in the Standard Model. Discrepancies between measurements in the tree-level decays and decays with loop might provide evidence of the Physics Beyond the Standard Model. Results of the recent analysis of $B^0 \rightarrow D^0 K^{*0}$, $B_s^0 \rightarrow D_s^\pm K^\pm \pi^\pm \pi^\mp$, $B^\pm \rightarrow Dh^\pm$ and $B^- \rightarrow D^* K^-$ decays are presented in this paper. A new combination of all LHCb measurements is also discussed. Achieved precision of the LHCb result: $67 \pm 4^\circ$ dominates the world average.

Keywords: High-energy physics; LHCb; CERN; LHC; B mesons; rare decays; CPV.

DOI: <https://doi.org/10.31349/SuplRevMexFis.3.0308057>

1. Introduction

In the Standard Model of particle physics, the Cabibbo-Kobayashi-Maskawa matrix (CKM) [1] is a unitary matrix that describes the strength of the flavour-changing weak interaction. A series of equations is constructed from the unitarity condition of the CKM matrix. These equations have a graphic representation as triangles (Unitarity Triangles) on the complex plane, and the angles of these triangles are the CKM matrix parameters. The CKM angle $\gamma = \arg(-V_{ud}V_{ub}/V_{cd}V_{cb})$ is one of the least explored parameter of the CKM matrix. It can be measured through the interference of $b \rightarrow c$ and $b \rightarrow u$ quark transition amplitudes, which occur in the tree-level decays of B mesons.

Measurement of the CKM angle γ in tree-level processes is called *the standard candle* for the Standard Model because of very small theoretical uncertainty: $\Delta\gamma/\gamma < 10^{-7}$ [2]. Discrepancies between angle γ measured in processes with loops and tree-level only processes may provide strong evidence for the effects of Physics Beyond the Standard Model. Measurement of the CKM angle γ provided by the LHCb experiment is the most precise measurement of the CKM angle γ from a single experiment [3]. This measurement is a combination of a series of single measurements and the most precise one is obtained in the analysis of the $B^+ \rightarrow DK^+$ decay, where D stands for a superposition of D^0 and \bar{D}^0 mesons re-

constructed from the same final state [3]. However, extended studies of other $B \rightarrow DK$ type channels, including decays through resonant states, increase the precision of the γ measurement.

1.1. LHCb detector

The LHCb detector is a single-arm forward spectrometer. It covers the pseudorapidity range $2 < \eta < 5$ (pseudorapidity is related to the angle between particles three-momentum and the direction of the beam axis). The program of the LHCb experiment revolves around hadrons with b or c quarks. The detector is composed of several subsystems. Tracking detectors before and after 4 Tm dipole magnet allow reconstruction of the particle momentum with a relative uncertainty about 0.5% for low momentum and 1.0% for high momentum (> 200 GeV/c). The Impact Parameter resolution (the minimum distance of a particle track to primary vertex - PV, proton-proton interaction point) is $(15 + 29/p_T) \mu\text{m}$ (p_T is transverse momentum). The two ring-imaging Cherenkov (RICH) detectors, hadron and electron calorimeters identify particles. Muons are identified in muons chambers which are situated at the end of the LHCb spectrometer. The decay time resolution of $\tau \approx 45$ fs enables a measurement oscillations of neutral particles, especially B_s^0 and B_d^0 mesons. The details of the LHCb spectrometer (Fig. 1) with the description of all main subsystems can be found in Ref. [4].

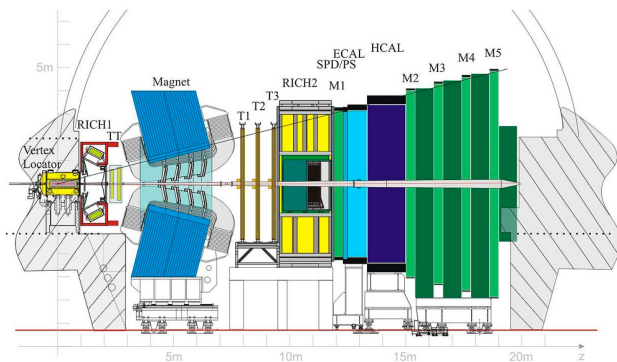


FIGURE 1. The scheme of the LHCb spectrometer [4].

2. Analysis of $B^0 \rightarrow D^0 K^{*0}$ decay

In the $B^0 \rightarrow D^0 K^{*0}$ decay, the K^{*0} stands for $K^{*0}(892)$ resonance reconstructed from $K^+\pi^-$ final state [5]. In both $B^0 \rightarrow D^0 K^{*0}$ and $B^0 \rightarrow \bar{D}^0 K^{*0}$ decays, there are colour-suppressed quark transitions. Colour suppression results in a small branching fraction of these decays; however, it enhances the interference effect and increases the γ sensitivity. A data set corresponding to 3.0 fb^{-1} and 1.8 fb^{-1} of integrated luminosity collected at centre-of-mass energies of 7-8, and 13 TeV, respectively, was collected during Run 1, 2015 and 2016. The CKM angle γ is measured using the GLW

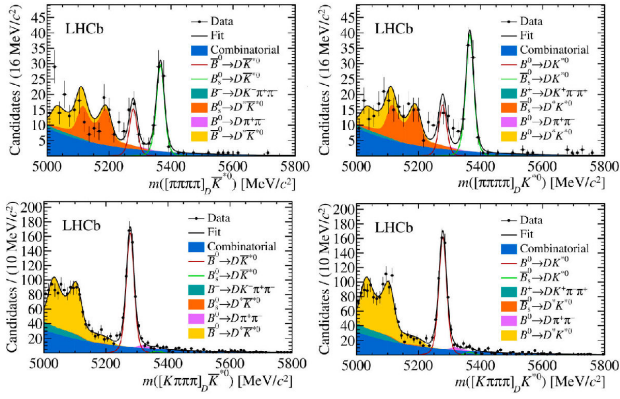


FIGURE 2. Invariant-mass distributions (black dots) with fit (lines and coloured areas) for the four-body GLW modes (top) and four-body ADS modes (bottom).

methods [6] for decays modes with D^0 meson decaying to CP eigenstate: $K^\pm K^\mp$ or $\pi^\pm \pi^\mp$ with the extension to $\pi^\pm \pi^\mp \pi^+ \pi^-$ and the ADS methods [7] for modes with D^0 meson decaying to $K^\mp \pi^\pm \pi^+ \pi^-$. The Gradient Boosted Decision Trees (BDT) algorithms were used to improve the separation of combinatorial background and signal. The set of algorithms was trained for each decay mode (one for two-body ADS modes, one for four-body ADS mode, and one for each GLW mode). The number of vetos was applied to reduce combinatorial and physical background contributions.

Invariant-mass distributions with fits for four-body ADS and GLW modes are shown in Fig. 2. Fits include several contributions: signal of $B^0 \rightarrow D^0 K^{*0}$ and $\bar{B}^0 \rightarrow D^0 K^{*0}$, combinatorial background described by an exponential function, partially reconstructed background from $B^0 \rightarrow D^{*0} K^{*0}$ where pion or γ from D^{*0} is missing, partially reconstructed background from $B^+ \rightarrow DK^+ \pi^+ \pi^-$ where one of the pions is not reconstructed and $B^0 \rightarrow D\pi^+ \pi^-$, where one of the pions is misidentified as kaon.

CP asymmetries evaluated in this analysis are compatible with zero within two standard deviations [5]. The global χ^2 minimization allows interpretation of these results in terms of $r_B^{DK^{*0}}$, γ and $\delta_B^{DK^{*0}}$. Figure 3 shows the contour

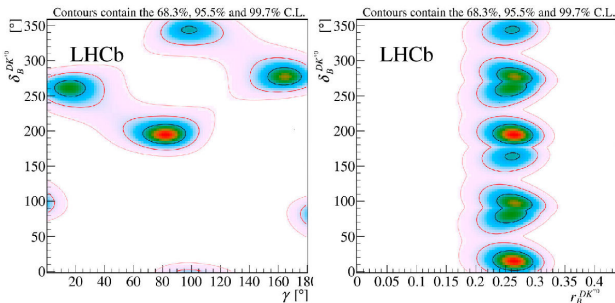


FIGURE 3. Result of the 2D scans of $\delta_B^{DK^{*0}}$ vs. γ (left) and $\delta_B^{DK^{*0}}$ vs. $r_B^{DK^{*0}}$ (right) with contour corresponding to 68.6%, 95.5% and 99.7% C.L., respectively.

for each pairs of parameters with 68.6%, 95.5% and 99.7% confidence levels (C.L.), respectively. The visible degeneracy can be broken by combining the result of this analysis with other LHCb analyses [3].

3. Analysis of $B_s^0 \rightarrow D_s^\pm K^\pm \pi^\pm \pi^\mp$ decay

Measurement of the CKM angle γ with $B_s^0 \rightarrow D_s^\pm K^\pm \pi^\pm \pi^\mp$ decay is an example of time-dependent studies at LHCb [8,9]. The full Run 1 and 2 LHCb data set (a 9 fb^{-1}) collected at centre-of-mass energies of 7, 8, and 13 TeV was used. This analysis consists of two independent measurements of the CKM angle γ . In the time-independent studies, the phase-space integrated decay-time spectrum is analysed. In the time-dependent approach, the strong-phase variation of the phase space of the decay is taken into account. The $B_s^0 \rightarrow D_s^\pm \pi^\pm \pi^\pm \pi^\mp$ is used to calibrate the detector's effects and to measure the $B_s^0 - \bar{B}_s^0$ mixing frequency - another parameter of the CKM matrix which is a difference between mass eigenstates of B_s^0 meson.

Selection of the candidates require the information from the particle identification system, B_s^0 meson proper time and displace of B_s^0 vertex from PV. The BDT algorithm was used to suppress the combinatorial background. Invariant mass distributions of $B_s^0 \rightarrow D_s^\pm \pi^\pm \pi^\pm \pi^\mp$ and $B_s^0 \rightarrow D_s^\pm K^\pm \pi^\pm \pi^\mp$ with fit are shown in Fig. 4.

The $B_s^0 \rightarrow D_s^\pm \pi^\pm \pi^\pm \pi^\mp$ candidates were used in the calibration of taggers of flavour tagging algorithms [10] which aim was to determine the flavour of the B_s^0 meson produced in the proton-proton collisions. There are two complementary methods: the opposite-side (OS) tagger and the same-side (SS) tagger. The same-side (SS) tagger exploits the kaon charge produced together with the B_s^0 meson in the fragmentation process. Opposite Side (OS) tagger exploits the decay products of the other b hadron (b hadrons are always produced in $b\bar{b}$ pairs): lepton (electron or muon) from semileptonic B decays or kaon from $b \rightarrow c$ and $b \rightarrow s$ processes. Each algorithm provides a decision for each candidate and tagging efficiencies.

Figure 5-left presents the proper-time spectrum for tagged B_s^0 candidates. The mixing asymmetry for $B_s^0 \rightarrow D_s^\pm K^\pm \pi^\pm \pi^\mp$ candidates is shown on Fig. 5-right. The result of measurement of $B_s^0 - \bar{B}_s^0$ mixing frequency is:

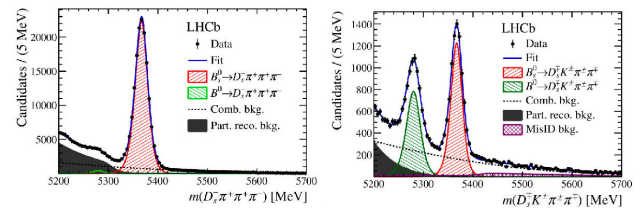


FIGURE 4. Invariant mass distributions for $B_s^0 \rightarrow D_s^\pm \pi^\pm \pi^\pm \pi^\mp$ candidates (left) and $B_s^0 \rightarrow D_s^\pm K^\pm \pi^\pm \pi^\mp$ (right) with the fit.

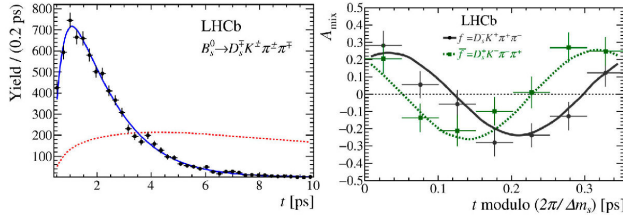


FIGURE 5. Background-subtracted decay-time distribution of $B_s^0 \rightarrow D_s^\pm K^\pm \pi^\pm \pi^\mp$ candidates (left) and mixing asymmetry along with the model-independent fit projections (right).

$$\Delta m_s = (17.757 \pm 0.007 \pm 0.008) \text{ ps}^{-1},$$

where the first uncertainty is statistical and the second systematic.

Results of measurement of the CKM angle γ in the phase-space-integrated analysis are presented below. The CP coefficients (detailed definitions in Ref. [9]) C_f , $A_f^{\Delta\Gamma}$, $A_{\bar{f}}^{\Delta\Gamma}$, S_f and $S_{\bar{f}}$ evaluated in this analysis:

$$C_f = 0.631 \pm 0.096 \pm 0.032$$

$$A_f^{\Delta\Gamma} = -0.334 \pm 0.232 \pm 0.097$$

$$A_{\bar{f}}^{\Delta\Gamma} = -0.695 \pm 0.215 \pm 0.081$$

$$S_f = -0.424 \pm 0.135 \pm 0.033$$

$$S_{\bar{f}} = -0.463 \pm 0.134 \pm 0.031$$

can be converted into the parameters: $\gamma - 2\beta_s$, r , κ and δ .

The full phase-space spectrum comprises resonances that potentially contribute to the $B_s^0 \rightarrow D_s^\pm K^\pm \pi^\pm \pi^\mp$ decay. The

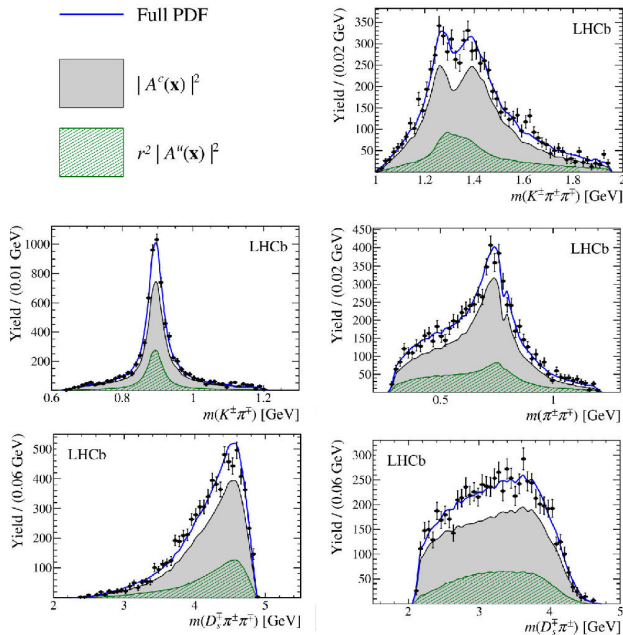


FIGURE 6. Invariant mass distributions for $B_s^0 \rightarrow D_s^\pm K^\pm \pi^\pm \pi^\mp$ candidates with the fit and indication of contribution from $b \rightarrow c$ and $b \rightarrow u$ decays amplitudes.

two quasi-independent models describe the $b \rightarrow c$ and $b \rightarrow u$ type decays. Ideally, the model should provide a good description of the invariant mass distributions and keep the number of included contributions as small as possible. The model complexity is limited using the LASSO technique.

The Fig. 6 presents the invariant-mass distribution of background-subtracted $B_s^0 \rightarrow D_s^\pm K^\pm \pi^\pm \pi^\mp$ candidates with the fits from the model for $b \rightarrow c$ and $b \rightarrow u$ type contributions. The summary of measurements of the CKM matrix parameters, including the CKM angle γ with model-independent and model-dependent methods is presented below:

Parameter	Model-independent	Model-dependent
r	$0.47^{+0.08+0.02}_{-0.08-0.03}$	$0.56 \pm 0.05 \pm 0.04 \pm 0.07$
κ	$0.88^{+0.12+0.04}_{-0.19-0.07}$	$0.72 \pm 0.04 \pm 0.06 \pm 0.04$
δ	$(-6^{+10+2}_{-12-4})^\circ$	$(-14 \pm 10 \pm 4 \pm 5)^\circ$
$\gamma - 2\beta_s$	$(42^{+19+6}_{-13-2})^\circ$	$(42 \pm 10 \pm 4 \pm 5)^\circ$

4. Analysis of $B^\pm \rightarrow Dh^\pm$ decay

The LHCb collaboration performed the model-independent study of the $B^\pm \rightarrow DK^\pm$ and $B^\pm \rightarrow D\pi^\pm$ decay with $D \rightarrow K_S^0 \pi^+ \pi^-$ or $D \rightarrow K_S^0 K^+ K^-$ using the GGSZ method [11]. The full LHCb Run 1 and 2: 9 fb^{-1} of data collected at centre-of-mass energies of 7, 8, and 13 TeV has been exploited [12]. Because the K_S^0 mesons may decay inside or outside the VELO detector, K_S^0 mesons are reconstructed in several different ways. The K_S^0 mesons reconstructed from *long* tracks decay inside the VELO and have a better track, mass and momentum resolution than K_S^0 reconstructed from *downstream* type tracks outside the VELO detector. The significantly higher number of downstream types K_S^0 mesons compensates for the worse quality of downstream tracks; however, it implies the additional selection of these tracks.

The combinatorial background is suppressed by the BDT algorithms. In the analysis of $B^\pm \rightarrow Dh^\pm$ decay, two different BDT algorithms were trained. One for selection of events with K_S^0 reconstructed from long tracks, and another for events with K_S^0 reconstructed from the downstream track. The BDT classifier rejected approximately 98% of background events and only 7% of signal events in the validation sample.

The invariant mass distributions for the $B^\pm \rightarrow DK^\pm$, $B^\pm \rightarrow D\pi^\pm$ with $D \rightarrow K_S^0 \pi^+ \pi^-$ or $D \rightarrow K_S^0 K^+ K^-$ for a different type of tracks with the fit are presented in Fig. 7. The Dalitz plots for the signal region (events with B^\pm meson mass within $30 \text{ MeV}/c^2$ mass windows around nominal B -meson mass) are shown in Fig. 8. Four different binning schemes are available to measure the c_i and s_i parameters. The binning schemes are created assuming a strong-phase difference distribution. This assumption is based on BaBar

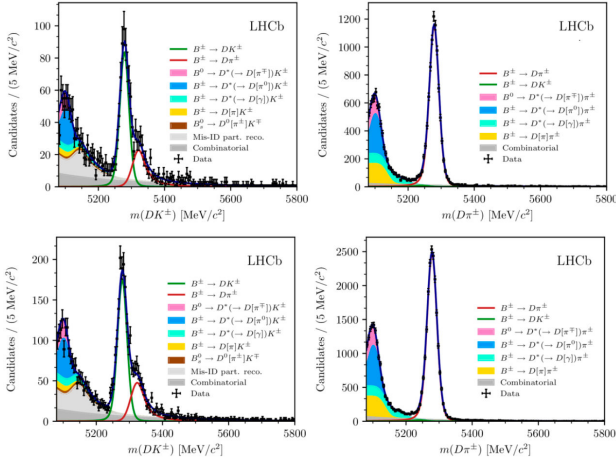


FIGURE 7. Invariant mass distributions for the $B^\pm \rightarrow DK^\pm$ (left) and $B^\pm \rightarrow D\pi^\pm$ (right) with $D \rightarrow K_S^0 K^+ K^-$ (K_S^0 long - top, K_S^0 downstream - bottom).

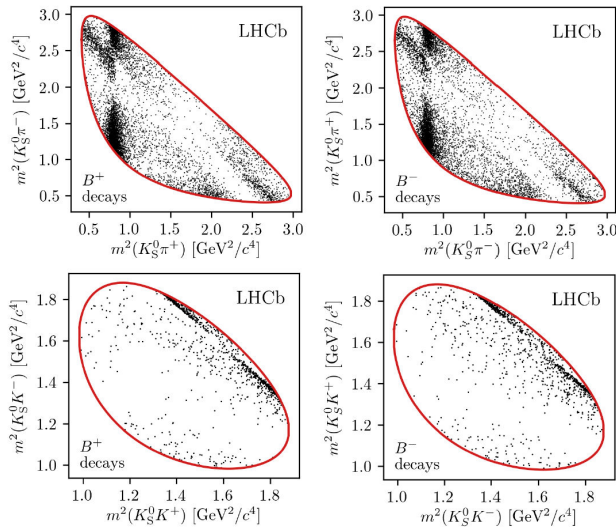


FIGURE 8. Dalitz plot for $B^+ \rightarrow DK^+$ (left) and $B^- \rightarrow DK^-$ (right) in the signal region, with $D \rightarrow K_S^0 \pi^+ \pi^-$ (top) and $D \rightarrow K_S^0 K^+ K^-$ (bottom).

model [13]. The optimal binning schemes for $D^0 \rightarrow K_S^0 \pi^+ \pi^-$ and $D^0 \rightarrow K_S^0 K^+ K^-$ are presented in Fig. 9.

The results for x_{\pm}^{DK} , y_{\pm}^{DK} and the CKM angle γ are presented in Fig. 10. The results are given with C.L. at 68.3% and 95.5%.

The CP observables are interpreted in terms of CKM angle γ , δ_B and r_B ratio. The results of measurement are:

Parameter	Result
γ	$(68.7^{+5.2}_{-5.1})^\circ$
$r_B^{DK^\pm}$	$0.0904^{+0.0077}_{-0.0075}$
$\delta_B^{DK^\pm}$	$(118.3^{+5.5}_{-5.6})^\circ$
$r_B^{D\pi^\pm}$	0.0050 ± 0.0017
$\delta_B^{D\pi^\pm}$	$(291^{+24}_{-26})^\circ$

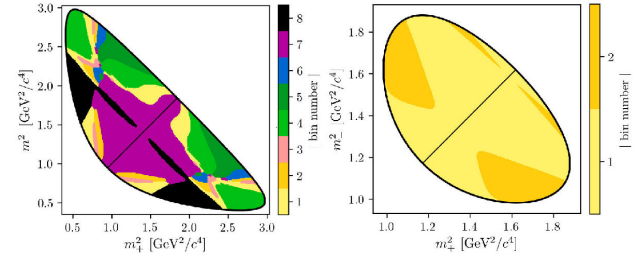


FIGURE 9. Binning schemes for $D^0 \rightarrow K_S^0 \pi^+ \pi^-$ decays (left) and $D^0 \rightarrow K_S^0 K^+ K^-$ decays (right). The black diagonal line separate positive and negatives bins.

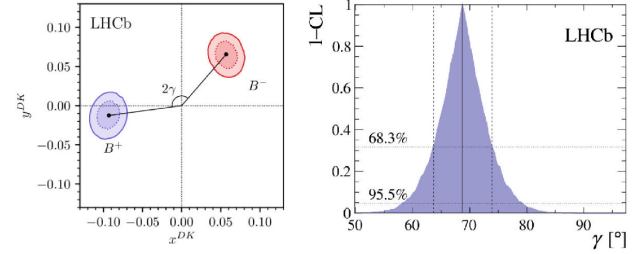


FIGURE 10. The 68.3% and 95.5% C.L. contour for x_{\pm}^{DK} and y_{\pm}^{DK} (left), the C.L. for the CKM angle γ (right).

This measurement of the CKM angle γ is the most precise determination of γ at LHCb.

5. Analysis of $B^- \rightarrow D^* K^-$

Analysis of $B^- \rightarrow D^* K^-$ decay is the example of the extension of $B \rightarrow DK$ decays studies over resonant states [14]. In this decay, the vector D^* meson decay to $D(\gamma/\pi^0)$ final state. The D meson decay to CP -even $D \rightarrow K^+ K^-$ or $D \rightarrow \pi^+ \pi^-$ final state or non- CP $D \rightarrow K^+ \pi^+$. It enables the measurement of the CKM angle γ using GLW and ADS methods.

The $B^- \rightarrow D^* K^-$ decay was partially reconstructed with the inclusion of γ or π^0 . This is the first analysis of this type at LHCb. The main advantage of partially reconstructed studies comes from significantly larger yields. Because the efficiency of the reconstruction of the neutral particle at LHCb is lower than charged particles, the number of full reconstructed candidates is significantly lower.

The data sample was collected during proton-proton collisions at centre-of-mass energies of 7, 8, and 13 TeV corresponds to 5.7 fb^{-1} . Events selection based on the requirement of D^0 meson mass within 25 MeV/c^2 mass window around the nominal mass of D^0 meson. The main components of the selection included the particle identification and BDT algorithm. The BDT was trained using a simulation sample of $B^- \rightarrow D^* K^-$ events and data sample containing events with B^- candidates mass above 5900 MeV/c^2 . The Fig. 11 show invariant-mass distribution of $B^\pm \rightarrow [K^\pm \pi^\pm]_D h^\pm$ candidates. The fit includes 16 contributions from the signal, physical background, combinatorial background, misidentification and more.

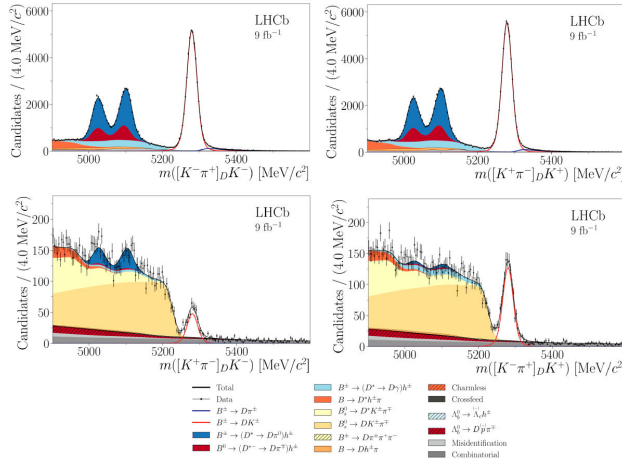


FIGURE 11. Invariant-mass distribution of $B^\pm \rightarrow [K^\pm\pi^\pm]_D h^\pm$ candidates with fit.

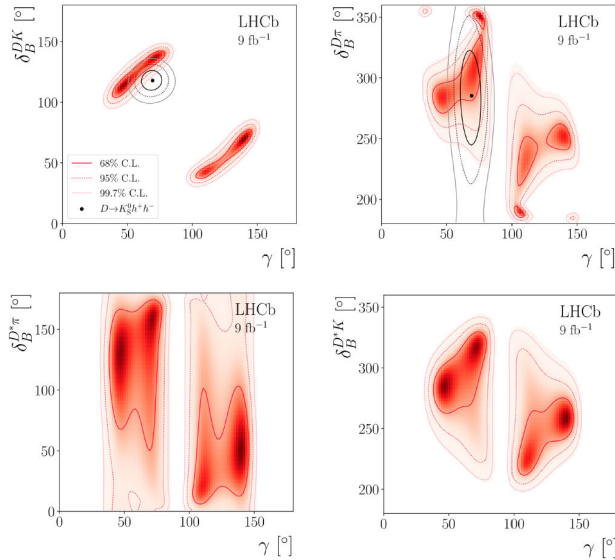


FIGURE 12. Confidence regions for the CKM angle γ vs. other CKM matrix parameters: $\delta_B^{DK/\pi}$, and $\delta_B^{D^*K/\pi}$.

The result of the analysis is over 28 of CP observables [12]. The CKM angle γ has not been measured directly in this analysis, however the CP observables provide an input to profile likelihood contours of the CKM matrix parameters: γ , $r_B^{DK/\pi}$, $\delta_B^{DK/\pi}$, $r_B^{D^*K/\pi}$ and $\delta_B^{D^*K/\pi}$. The profile likelihood contours for the CKM angle γ and other parameters at 68%, 95%, and 99.7% C.L. are shown in Fig. 12.

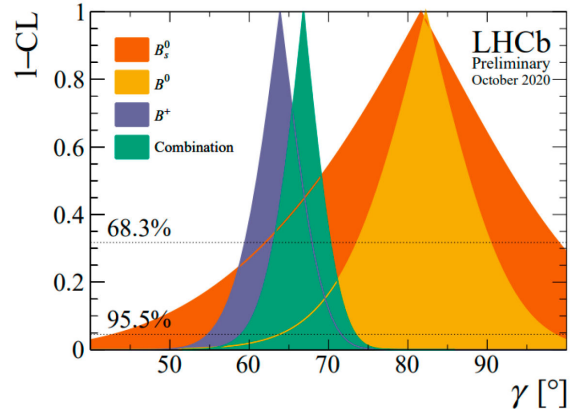


FIGURE 13. The 1-CL scan of the CKM angle γ for combination and for decays with different initial B state.

6. The CKM angle γ combination and conclusions

The LHCb combination includes results of analysis of 16 decay modes using methods described in this paper. From the last combination in 2018 [18], there are two new ($B_s^0 \rightarrow D_s^\mp K^\pm \pi^\pm \pi^\mp$ and $B \rightarrow DK^*$) and five updated results. The full list of contributions can be found in Ref. [3]. The LHCb collaboration provides the CKM angle γ measurement split by the initial B state and the combination (Fig. 13) [3]:

Configuration	68.3% C.L.	95.4% C.L.
Combination	$(67 \pm 4)^\circ$	$(67_{-8}^{+7})^\circ$
B^+	$(64_{-5}^{+4})^\circ$	$(64_{-9}^{+8})^\circ$
B^0	$(82_{-9}^{+8})^\circ$	$(82_{-19}^{+16})^\circ$
B_s^0	$(82_{-20}^{+17})^\circ$	$(82_{-39}^{+24})^\circ$

Analyses of the full Run 1 and Run 2 data from LHCb provide significant improvement in reducing the uncertainty of the CKM angle γ . The LHCb result: $\gamma = 67 \pm 4^\circ$ is in excellent agreement with the result from the CKMfitter group: $(65.7_{-2.7}^{+0.9})^\circ$ [16] and UTfit collaboration: $(65.8 \pm 2.2)^\circ$ [17]. LHCb also performed the single most accurate measurement of the CKM angle γ : $\gamma = (68.7_{-5.1}^{+5.2})^\circ$ [12]. Improvement of measurement precision of the CKM angle γ may provide compelling evidence of physics beyond the Standard Model.

Acknowledgments

This research was supported in part by National Research Centre, Poland (NCN) and grant No. UMO-2018/31/N/ST2/01471.

1. N. Cabibbo, Unitary Symmetry and Leptonic Decays. *Phys. Rev. Lett.* **10** (1963) 531, <https://doi.org/10.1103/PhysRevLett.10.531>.
2. J. Brod and J. Zupan, The ultimate theoretical error on from $B \rightarrow DK$ decays. *Journal of High Energy Physics* **2014** (2014). [https://doi.org/10.1007/jhep01\(2014\)051](https://doi.org/10.1007/jhep01(2014)051).
3. Aaij *et al.* Updated LHCb combination of the CKM angle. (2020). <https://cds.cern.ch/record/2743058>.
4. Aaij *et al.* LHCb Detector Performance. *Int. J. Mod. Phys. A*, **30** (2014) 73. <https://doi.org/10.1142/S0217751X15300227>.
5. Aaij *et al.* Measurement of CP observables in the process $B^0 \rightarrow DK$ with two- and four-body D decays. *JHEP*, **1908** (2019) 30. [https://doi.org/10.1007/JHEP08\(2019\)041](https://doi.org/10.1007/JHEP08(2019)041).
6. M. Gronau and D. Wyler, On determining a weak phase from charged B decay asymmetries. *Phys. Lett. B*, **265** (1991) 172, [https://doi.org/10.1016/0370-2693\(91\)90034-N](https://doi.org/10.1016/0370-2693(91)90034-N).
7. D. Atwood, I. Dunietz, and A. Soni, Improved methods for observing CP violation in $B \rightarrow KD$ and measuring the CKM phase. *Phys. Rev. D*, **63** (2001) 036005, <https://doi.org/10.1103/physrevd.63.036005>.
8. R. Fleischer, New strategies to obtain insights into CP violation through and decays. *Nuclear Phys. B* **671** (2003) 459. <https://doi.org/10.1016/j.nuclphysb.2003.08.010>.
9. Measurement of the CKM angle γ and $B_s^0 \rightarrow B_s^0$ mixing frequency with $B_s^0 \rightarrow D_s^\mp h^\pm \pi^\pm \pi^\mp$ decays. *JHEP* **2103** (2020) 46, [https://doi.org/10.1007/JHEP03\(2021\)137](https://doi.org/10.1007/JHEP03(2021)137).
10. D. Fazzini, Flavour Tagging in the LHCb experiment. *PoS, LHCP* **2018** (2018) 7. <https://doi.org/10.22323/1.321.0230>.
11. A. Giri, Y. Grossman, A. Soffer, and J. Zupan, Determining γ using $B^\pm DK^\pm$ with multibody D decays. *Phys. Rev. D*, **68** (2003) 054018. <https://doi.org/10.1103/physrevd.68.054018>.
12. Aaij *et al.* Measurement of the CKM angle γ in $B^\pm \rightarrow DK^\pm$ and $B^\pm \rightarrow D\pi^\pm$ decays with $B^\pm \rightarrow K_S^0 h^+ h^-$. *J. High Energy Physics* **2021** (2021). [https://doi.org/10.1007/jhep02\(2021\)169](https://doi.org/10.1007/jhep02(2021)169).
13. P. del Amo Sanchez *et al.* Evidence for direct CP violation in the measurement of the Cabibbo-Kobayashi-Maskawa angle gamma with $B_\pm \rightarrow D^{(*)} k^{(*)\pm}$ decays. *Phys. Rev. Lett.*, **105** (2010) 121801. <https://doi.org/10.1103/PhysRevLett.105.121801>.
14. R. Aaij *et al.* Measurement of CP observables in $B^\pm \rightarrow D^{(*)} K^\pm$ and $B^\pm \rightarrow D^{(*)} K^{(*)\mp}$ decays using twobody D final states. *JHEP*, **2104** (2020) 36. [https://doi.org/10.1007/JHEP04\(2021\)081](https://doi.org/10.1007/JHEP04(2021)081).
15. Aaij *et al.*, Update of the LHCb combination of the CKM angle. Technical report, CERN, Geneva, May 2018. <https://cds.cern.ch/record/2319289>.
16. J. Charles *et al.*, Current status of the standard model CKM fit and constraints on $\Delta F = 2$ new physics. *Phys. Rev. D* **91** (2015). <https://doi.org/10.1103/physrevd.91.073007>.
17. M. Bona *et al.*, The unitarity triangle fit in the standard model and hadronic parameters from lattice QCD: a reappraisal after the measurements of Δm_s and $BR(B \rightarrow \tau\mu\tau)$. *J. High Energy Physics*, **2006** (2006) 081. <https://doi.org/10.1088/1126-6708/2006/10/081>.